Title

1

4

5

11

- 2 Murder in cold blood? Forensic and bioarchaeological identification of the skeletal remains of
- 3 Béla, Duke of Macsó (c. 1245–1272)

Authors

- 6 Tamás Hajdu^{1,2*}, Noémi Borbély^{3,4*}, Zsolt Bernert⁵, Ágota Buzár⁵, Tamás Szeniczey¹, István
- Major⁶, Claudio Cavazzuti⁷, Mihály Molnár⁶, Anikó Horváth⁶, László Palcsu⁶, Barna Árpád
- 8 Kelentey⁸, János Angyal⁹, Balázs Gusztáv Mende³, Kristóf Jakab³, Zsuzsa Lisztes-Szabó⁶,
- 9 Ágoston Takács¹⁰, Olivia Cheronet¹¹, Ron Pinhasi¹¹, David Emil Reich^{12,13,14,15}, Martin
- 10 Trautmann¹⁶*, Anna Szécsényi-Nagy³*

12 Affiliations

- ¹Department of Biological Anthropology, Faculty of Science, Eötvös Loránd University,
- 14 Budapest, Hungary.
- ²Centre for Applied Bioanthropology, Institute for Anthropological Research, Zagreb, Croatia.
- ³Institute of Archaeogenomics, HUN-REN Research Centre for the Humanities, Budapest,
- 17 Hungary.
- ⁴Doctoral School of Biology, Institute of Biology, ELTE Eötvös Loránd University, Budapest,
- 19 Hungary.
- ⁵Department of Anthropology, Hungarian Natural History Museum, Budapest, Hungary.
- ⁶Isotope Climatology and Environmental Research Centre, HUN-REN Institute for Nuclear
- 22 Research, Debrecen, Hungary.
- ⁷Department of History and Culture, Alma Mater Studiorum, University of Bologna, Bologna,
- 24 Italy.
- 25 *Department of Operative Dentistry and Endodontics, Faculty of Dentistry, University of
- 26 Debrecen, Debrecen, Hungary.
- ⁹Department of Periodontology, Faculty of Dentistry, University of Debrecen, Debrecen,
- 28 Hungary.
- 29 ¹⁰Medieval Department, Castle Museum Budapest History Museum, Budapest, Hungary.
- 30 ¹¹Department of Evolutionary Anthropology, University of Vienna, Vienna, Austria.
- ¹²Department of Genetics, Harvard Medical School, Boston, USA.
- 32 ¹³Department of Human Evolutionary Biology, Harvard University, Cambridge, MA, USA.
- ¹⁴Broad Institute of MIT and Harvard, Cambridge, MA, USA.
- 34 ¹⁵Howard Hughes Medical Institute, Boston, MA, USA.
- 35 ¹⁶Department of Cultures/Archaeology, University of Helsinki, Helsinki, Finland.

***Corresponding authors:**

- Tamás Hajdu, e-mail: tamas.hajdu@ttk.elte.hu; https://orcid.org/0000-0002-3604-1125
- Noémi Borbély, e-mail: borbely.noemi@abtk.hu; https://orcid.org/0000-0002-1488-5298
- 40 Martin Trautmann, e-mail: ao.anthropologie@googlemail.com; https://orcid.org/0000-0003-0057-
- 41 6563

Anna Szécsényi-Nagy, e-mail: szecsenyi-nagy.anna@abtk.hu; https://orcid.org/0000-0003-2095-738X

Abstract

42 43

4445

46

47

48 49

50

51

52

53

54

55

56

57

58

59

60

61 62

63

64

65 66

67

68

69

70

71

72

73

74

75

76

77

78

80

81

82

83

84

85

86

87

88

89

90

In 1915, the remains of a male were discovered in a 13th-century monastery on Margaret Island, Budapest. Historical context suggested that the remains may belong to Duke Béla of Macsó (c. 1245–1272), grandson of King Béla IV of Hungary (House of Árpád) and son of Duke Rostislav (Rurik dynasty). We applied a complex approach to identify the individual and reconstruct the circumstances of his death. Radiocarbon dating, when adjusted for freshwater reservoir effects linked to a high-protein diet, placed the burial in the mid-13th century. Skeletal features corresponded to a young adult male. Stable isotope and dental calculus analyses indicated a high-status diet rich in animal proteins and C3 cereals. Ancient DNA confirmed descent from King Béla III (Árpád dynasty) and Ychromosomal affiliation with the Rurikid lineage. Forensic evidence revealed 26 perimortem injuries, suggesting a coordinated, premeditated assassination involving at least three assailants. The pattern of injuries indicates both planning and intense emotional involvement. Our findings provide the first genetic identification of a medieval royal, and resolve a century-old archaeological question, and illustrate the power of integrating multidisciplinary methods to confirm historical hypotheses and reconstruct violent deaths from the past with unprecedented detail.

Teaser

With unprecedented details, this study shows the impact of integrating multidisciplinary methods to confirm historical hypotheses and reconstruct violent deaths from the past.

Introduction

Historical and archaeological background

Béla (c. 1245–1272), Duke of Bosnia and Macsó, was the second son of Princess Anna (1226-c 1274; daughter of King Béla IV of Hungary) and Rostislav (1219-1263) of the Rurik dynasty, Prince of Halych. Duke Béla first appeared on the political scene in 1265, when his mother, Princess Anna, a supporter of King Béla IV (reigned (r. 1235-1270), launched a war against his brother, the younger king Stephen V. The war was led by Duke Béla of Macsó, who was around 20 years old at the time (1). His army suffered a devastating defeat, after which Béla IV made peace with the younger king Stephen V. In 1270, after the death of Béla IV, Princess Anna fled to her son-in-law, King Ottokar II of Bohemia, who then invaded Hungary. However, King Stephen V and Duke Béla repelled Ottokar and forced him to make peace. Duke Béla's support for Stephen V stabilized the duke's political position, but it changed after the unexpected death of King Stephen V in 1272. In opposition to the underage Ladislaus, son of King Stephen V, some of the lords supported Duke Béla as a candidate for regent or even king. Despite this, in August 1272, Ladislaus was crowned as King Ladislaus IV. To resolve the conflict, Duke Béla was invited to a council at the nunnery on the Island of Hares in November. But instead of a council meeting, an assassination plot was arranged. Duke Béla was brutally massacred by the assembled pro-Ladislaus lords led by Henrik of the House of Héder (Henrik Kőszegi). With this unpunished act, not only was a potential pretender to the throne eliminated, but the vast estates of the childless duke were also seized and later redistributed among the king's supporters. The earthly remains of the slaughtered Béla were laid to rest by his relatives within the walls of the Dominican nunnery on the Island of Hares (now Margaret Island, Budapest) (1).

On the 6th of April 1915, archeological excavation of the Dominican nunnery on Margaret Island was initiated by K. Salkovics (2) (Supplementary Figure 1). Three graves were uncovered in the sacristy, one of which contained the visibly dismembered skeleton of a young man. Other sources describe the area between the kitchen and the so-called well-house as the site of the graves (3). In any case, it is certain that the graves were found in the 13th-century monastery building.

Previous biological anthropological investigations

After the excavation, L. Bartucz investigated the remains. Based on his unpublished results, the skeleton (Figure 1, Supplementary Figure 2). belonged to a 20-25-year-old male, and 23 cut-marks were observed on the bones. Bartucz supposed that the male had not died in a duel, but was attacked by multiple persons from several directions, and even after falling to the ground, his body was further mutilated. Based on Bartucz's theory, the remains belonged to Duke Béla of Macsó (4–5).

Bernert and Buzár published the preliminary results of the investigation of the postcranial bones without the detailed investigation of the skull. They estimated the male's age at death to be $23(\pm 1)$ years. They suggested that the male was probably first stabbed in the spine from behind, which may have forced him to the ground. He was then slashed by assailants from several directions: on his hands, legs, head, and trunk.

The aim of the study

Our study presents the results of a multidisciplinary analysis of the skeletal remains found in a Dominican nunnery on Margaret Island, aiming to reconstruct the circumstances of the individual's life and death and establish personal identification.

Results

Radiocarbon investigation

The collagen fraction of bone samples was prepared in multiple ways (n=7), yielding conventional ¹⁴C dates ranging from BP 874±19 to BP 922±17, corresponding to a summarized calibrated age range of approximately cal AD 1030-1230 at a 95.4% probability level (Supplementary Figure 3). We could not observe significant differences between the results obtained by the different pretreatment methods for the rib or skull fragments. Thus, a freshwater reservoir effect test, related to aquatic-derived food, was performed applying an age shifting of 50-150 yrs towards the younger calendar dates. The structural carbonate of the bioapatite fraction of a rib was also prepared and measured, resulting in a conventional age of BP 841±18 (AD 1170-1260 at 95.4% probability level).

Biological Anthropology

The transition analysis aging method integrates findings from 24 skeletal traits. The estimated age-at-death using cranial sutures, pubic symphysis, and auricular surface ranges between 19.8 and 30.9 years (95% confidence, corrected data), with a maximum likelihood estimate of 24.3 years. The determined sex (male) based on morphological traits of the cranium (Figure 1) as well as the metric characteristics of the pelvic bone, corresponds with the genetic sex. The estimated stature of the individual was 178.8 cm, based on the average femoral length.

Slight marginal osteophytes can be seen in both knee joints, on both condyles of the left femur and right tibia. Slight hypertrophy of the subchondral bone $(5.7 \times 3.9 \text{ mm})$ can be seen on the medial side of the right patellar articular surface. Slight marginal bone "lipping" is visible on the upper articular processes of the 4th-9th thoracic vertebrae. The

insertion sites of the muscles and tendons are slightly expressed on the tuberosity of the right radius, on the deltoid tuberosity of both humeri, on the linea aspera of left femur, and on the soleal line of both tibiae. The lateral and anterior surface of the vertebral bodies are hypervascularized. Healed mild periosteal lesions appeared on the medial surface of the mid-third part of both tibiae, and on the mid-third part of the left fibula.

Odontology

Eight teeth are intact and properly positioned in the mandible, surrounded by healthy periodontal bone. Upper left 1st premolar and 1st-2nd molars are fractured in the region of the tooth neck, presumably due to forced impact immediately before death. The plane of fracture of the two molars is the same as the plane of the cut of the zygomatic bone, the zygomatic process of the maxilla and the vestibular bony process of the upper jaw around those molars (Supplementary Figure 4A-B). The roots of the broken teeth and the bone around them are intact, free from signs of inflammation, which rules out the possibility of an antemortem fracture due to tooth disease. The lack of periapical lesions around the roots of the fractured teeth suggests that the person died directly after the incident. A non-dislocated fracture of the mesiobuccal root of the left upper first molar tooth was also observed (Supplementary Figure 4C).

Dental calculus analysis

Presumably, due to the individual's young age, the amount of calculus was not particularly high (14.3 mg). 791 microphotographs were taken, showing more than one thousand microfossils. Microfossil remains found in dental calculus are usually difficult to quantify (6). It was estimated that 80% of the microfossil remains were microcharcoal, starch and miscellaneous unidentified plant and animal remains, with a smaller portion of fibers, phytoliths, pollen, animal and plant egg cells and spores, and fungal remains (Supplementary Figure 5). The size and shape of the starch granules predominantly suggest they came from the endosperm tissue of grains belonging to the Triticeae tribe, namely wheat (Triticum) and barley (Hordeum). In addition, several long plant hairs (trichomes) were detected that are characteristic of the wheat grains (Supplementary Figure 6). The starch grains' identifiability was limited because they bore marks of grinding, cooking, and baking (7). Regarding the size, morphological and light refraction characters of the starch grains and the material of the gelatinized starch in the dental calculus were similar to the reference material of the boiled wheat grits and the baked wheat bread (Supplementary Figure 6). Yeast cells may also have integrated into the calculus, but it cannot be established with certainty. In the sample of the individual's dental calculus, 17 pollen grains were detected, which is a large number (8), and numerous calcium oxalate crystals were found in the calculus matrix.

Forensic traumatological assessment

The assessment of the skeleton reveals 26 perimortem lesions (Figure 1-2) – nine on the skull (Figure 1-3, Supplementary Figures 7 and 8) and 17 on postcranial bones (Figure 2 and 4, Supplementary Figure 9-17) – all sustained in a single violent event (Supplementary Information 1). All wounds are clearly the result of intent and interpersonal aggression. Their characteristics suggest a coordinated assault involving probably three assailants.

One attacker approached from the front; the others were flanking the victim from the left and right. The injuries, primarily on the front of the body, imply the victim faced his attackers in an open confrontation. The presence of multiple defensive wounds on the forearms confirms he was aware of the attack and attempted to defend himself.

The weapons used can be identified as two different types of blades, probably saber and longsword (the detailed arguments are shown in Supplementary Information 2). The clean and deep cut marks, especially on the skull, suggest the victim was unarmored, as body armor or a helmet would have prevented such injuries.

The reconstruction of the assault sequence (Supplementary Information 3) indicates the attack began with saber strikes to the head and upper body, followed by defensive injuries as the victim attempted to block further blows. The attackers eventually incapacitated the victim with further strikes from the flanks, continuing the assault as he fell to the ground, and delivering fatal injuries to the head and face.

The intensity of the attack clearly indicates an intent to kill, while the numerous blows to the face suggest intense emotional involvement, such as rage or hate ("overkill"). However, the coordinated nature of the attack implies premeditation, suggesting this was at least partly a planned assassination.

Strontium, stable carbon and nitrogen isotope ratio

The enamel of two left lower molars (M1, M2) have been sampled in three points of the tooth surface: at the crown cusp, at the middle of the crown and at the enamel-root junction. Based on the measurement results of the Sr isotope ratios the 1st molar forms a group (mean: 0.710363 ± 0.000184), the 2nd molar forms a different group (0.709769 ± 0.000111) (Supplementary Figure 18). Strontium isotope values of the first molar show that Béla was born and spent his early childhood in a different geographic place, as where he was buried, characterized by more radiogenic values, such as the regions of Vukovar or Sirmia (9), which were part of the Banate of Macsó. However, the exact and certain localisation of the territory where the investigated male was born and spent his early childhood, is not possible because of methodological limitations. In the Carpathian Basin and surrounding territories, more regions have the same or very similar strontium isotope values (9). During late childhood, the subject moved to a different region, possibly in the hinterland of Budapest. The ⁸⁷Sr/⁸⁶Sr value measured on the rib appears compatible with the local baseline, although bone tends to undergo a diagenetic alteration and contamination with the depositional soil.

The stable C/N ratios of the prepared samples do not imply heavy contamination, so the stable isotope results (Supplementary Table 1) can be used in subsequent analyses. The d13C of -19.3‰ implies a primarily C3-type plant-based diet. The stable nitrogen isotopic result (d15N) of 11·8‰ is situated above the range 6-10‰, which is characteristic for humans consuming largely terrestrial plants and animals (10). It suggests that animal-, and possibly aquatic-derived protein might have made a notable contribution to the diet of this individual.

aDNA analysis

There are published genetic studies available from both the paternal Rurik side and the maternally related Árpád Dynasties. These allowed us to make comparisons at the wholegenome level and for Y-chromosomal and mitochondrial uniparental lineage. For our analyses of the Y-chromosomal paternal side, we included modern samples from the *Rurikid Family Tree DNA Project* (11) representing descendants of the Rurik Dynasty, as well as the whole-genome data of Prince Dmitry Alexandrovich (c. 1250–1294) (12), who was a Grand Prince of Vladimir (northeastern principality of the Rus) and an eighth-degree relative and contemporary of Béla of Macsó from the Rurik dynasty. Prince Dmitry Alexandrovich's great-grandfather (Vsevolod III, Rurik dynasty) had a son (Sviatoslav III, Rurik dynasty) who was the great-great grandfather of Béla of Macsó. Firstly, we

233

234

235

236

237

238239

240

241

242

243

244

245

246

247

248

249

250

251

252

253

254

255

256

257258

259

260

261

262

263

264

265

266

267

268

269

270

271

272

273

274

275

276

277

278

279

280

281

investigated the short tandem repeats (STRs) of the Y-chromosome. Three independent reactions resulted in an STR profile based on 13 Y-STR loci, which suggested that DNA sample BPDOM01 belonged to the N1a1-M46 haplogroup (nevgen.org). Further downstream subgroups can be anticipated from the STR matches detected with the Rurikids and based on Y-chromosomal SNPs from the whole-genome analysis, BPDOM01 most probably belonged to the subgroup N1a1a1a1a1a1a (N1a-L550, ISOGG 2020 Version: 15.73 (Supplementary Table 2). Based on publicly available Y chromosome STR data with the participants of the Rurikids Dynasty project, we selected those families (branches) that had members who shared the most STR alleles with the sample BPDOM01. A median-joining network analysis with these Rurikid branches was performed with Network 10.1.0.0 (Figure 5A). According to the database of the FamilyTreeDNAa's Rurikid Dynasty DNA Project (11), the 13 Y-STR profile of BPDOM01 has 24 exact matches among the tested descendants of the Rurikids and Varangian families. Furthermore, it has a perfect match with the anticipated Rurik prince's Y-STR profile (lived ca. 830–879 AD), who was a paternal ancestor of Béla of Macsó in 12 generations distance. Among the present-day descendants, members of the Rurikids, Rurikid Princes, Varangians - 'Rurikids closest cousins' and 'Proto-Rurikids', and Finno-Karelian Branches share all 13 STR from the typed 13 markers of BPDOM01. The sub haplogroups of these individuals belong to Y10931 (N1a1a1a1a1a1a1a7a3a~) and Y4339 (N1a1a1a1a1a1a7a~) both located downstream from L550 on the Y tree (Supplementary Figure 4). This has been confirmed by the Yleaf analysis of genomic data, the S431 derived marker defining the N-L550 haplogroup is covered by three reads. This haplogroup classification supports the theory that the BPDOM01 sample belongs to a descendant of the Rurik Dynasty. The strongest evidence of his Rurikid origin is provided by the whole-genome-based Y-chromosomal haplogroup classification of Prince Dmitry Alexandrovich, which is N1a1a1a1a1a1a1a1a7a3b~ (N-VL11 terminal SNP), consistent with our results.

The maternal line of BPDOM01 can be classified as the mitochondrial sub-haplogroup U3b3, with an average mitogenome coverage of 66X. No identical mtDNA haplotype to BPDOM01's lineage was detected in published datasets. The U3b3 haplogroup has its present-day highest frequency around the Black Sea. It appears in ca. 3-6% in Turkey, populations of the Caucasus and Iraq, Iran today (13). This mtDNA subgroup's earliest appearance in ancient databases is in Minoan Greece, Crete (1871 BC), the Late Bronze Age Levant (1276 BC; today's Jordan) and the Iron Age Armenia (526-494 BC) (14, 15). Further ancient samples with the same maternal sub haplogroup are known from the following regions and periods: Hungary (Püspökladány-Eperjesvölgy, 975-1075 AD), Poland (Piast dynasty, 1040 AD), Turkey (Byzantine culture, 1163 AD). The phylogenetic tree of all available U3b3 mitogenomes is shown in Figure 5B, with the closest matches being modern Armenian, Adygei, Lebanese and Druze sequences (Supplementary Table 3). The maternal grandmother of Béla was Maria Laskarina (c. 1206-1270), a daughter of the Byzantine Emperor Theodor I., and Anna Komnene Angelina (c. 1176-1212), who was the Empress of Nicaea and daughter of the Byzantine Empress Euphrosyne Doukaina Kamaterina (c. 1155-1211). The U3b3 lineage aligns with the here presented maternal genealogy leading to Euphrosyne Doukaina as a rare but widespread lineage from the Caucasus to the Near East, likely prevalent in the Early Medieval Anatolia and the Aegean - South-Pontic world, from which Béla's maternal ancestors came. We present the genome-wide single nucleotide polymorphism (SNP) data (545,606 SNP) covered) from 1240k SNP capture of BPDOM01 and comparative samples in a principal component analysis (PCA) (Figure 6A, Supplementary Table 4). For the PCA analysis,

ancient data were projected on the modern European genetic variation using the Human

Origin panel as a reference dataset (included in the AADR database) (16). BPDOM01 aligned closest to modern Greek, Turkish and Moldavian samples in the PC1-PC2 (principal components 1 and 2) space, slightly extending towards the southeastern populations, which are representative of the present-day Caucasian groups. The closest samples originate from the medieval era of today's Hungary and Romania and medieval/ early modern Italy.

282

283

284

285

286

287

288 289

290

291

292

293

294 295

296

297

298

299

300

301

302

303

304

305

306

307

308

309

310

311

312

313

314

315

316

317

318

319

320

321

322

323

324

325

326

327

328

329

330

331

To explore Béla of Macsó's genomic composition, we applied the fastNGSadmix software. The fastNGSadmix program is an efficient and reliable tool for determining admixture proportions from NGS data of a single individual. It utilizes genotype likelihoods for its analyses, comparing the input sample to a set of predefined reference populations. This method maintains high accuracy even at low sequencing depths and compensates for biases introduced by small reference populations (17). Similar to those presented in Vyas et al. (18), we used a custom panel of ancient 4th–8th-century reference individuals. This panel was constructed with a similar geographic distribution to the 1000G populations to form seven ancient panel groups, such as Western Europe, Sub-Saharan, East Mediterranean, North Africa, South Asia, East Asia, and Scandinavia as in the premade reference panel of the fastNGSadmix program. The results align with the presumed origin of Béla of Macsó, having Byzantine (Eastern Mediterranean) ancestry on the mother's side and Rurik (Scandinavian) ancestry on the father's side (Supplementary

Figure 6B) (17). Applying ancIBD, the identity-by-descent (IBD) tool of Ringbauer et al. (19), the genomes of Dmitry Alexandrovich and BPDOM01 share a total of 118 cM DNA fragments with the largest matching chunk over 43 cM (Supplementary Table 5, Figure 7A and B). This result confirms them to be at least eighth-degree relatives, consistent with the historically recorded kinship between Dmitry and Béla of Macsó. Besides the sample of Prince Dmitry Alexandrovich, we incorporated into our ancIBD analysis the whole-genome sequences of Béla of Macsó's maternal great-greatgrandfather, King Béla III (1148-1196) of Hungary from the Árpád dynasty, further samples from the Coronation Basilica in Székesfehérvár, and a sample from the herma (skull relic) of St. Ladislaus from the Árpád dynasty (c. 1040-1095) (20–22). The ancIBD analysis (Figure 7A and B) reveals that the examined BPDOM01 sample is a fourth-degree relative of King Béla III, and approximately twice as distant from St. Ladislaus (21, 22), which supports the hypothesis that he was Duke Béla of Macsó (Supplementary Table 5). In the ancIBD run, we verified the identity of the data labelled under the codes BelaIII and HU3B. The former is from the publication by Wang et al. (21), and the latter is from the publication by Varga et al. (22). These are two different samples, both originating from Béla III (see Supplementary Table 5). The ancIBD showed that the BPDOM01 sample is probably a fourth-degree relative on an avuncular line of the HU52 sample from the Arpád dynasty, found in the Coronation Basilica in Székesfehérvár. Considering the historical and genetic data, we conclude that the skeleton from grave III HU52 may have been identical to Prince Andrew of Halych, the son of King Andrew II. Following the rationale and terminology employed by Olasz et al. (20), we refer to the sample included in the present analysis as HU52, originating from Grave III of the Coronation Basilica in Székesfehérvár, given that the published sequence used in our study (Varga et al. 22) is also associated with this identifier. It is important to note, however, that this individual is not identical to the one labelled II/52 in the original excavation records of the basilica, who was identified as a fetal skeleton.

We applied a clinical variant calling and pigmentation analysis on sample BPDOM01 with the variant calling tool from PAPline (23). Through the 1240k SNP capture, altogether 32 pigmentation markers were captured and detected with a 3.7x average coverage. Overall

darker pigmentation and darker skin, no melanoma risk or sunburn sensitivity characterized BPDOM01 and freckles were not characteristic, possibly having brown curlier hair and light brown eyes. No disease-associated genotypes were identified through the examination of 925 clinical variants (see Supplementary Table 6).

Discussion

The radiocarbon results of bone collagen indicate an earlier date than the recorded murder of Duke Béla. However, the building in which the skeleton was found is part of the Dominican monastery on Margaret Island, which was founded only in 1259 AD. As the first buildings of the monastery were built between 1246-1255, the burial could not have taken place earlier than 1246. Our ¹⁴C measurements were conducted seven times on the collagen fraction of the bones, and verified by independent laboratories, and the results are consistent. As the younger age of the bioapatite fraction suggests, the discrepancy between the radiocarbon results and historical data can likely be explained by the effect of the individual's diet. Moreover, the higher d15N value also supports the possibility of reservoir effect shifting the real ¹⁴C age toward an older date (24, 25). Although the dental calculus microremain analysis results did not provide evidence of this type of diet, it cannot be ruled out that the level of ancient carbon in the diet was sufficiently high to influence the radiocarbon results, causing a reservoir effect of 100-200 years for the collagen fraction and 50-100 years for the structural carbonate of bioapatite. Since our genetic analysis confirms that the investigated male belonged to the highest level of society (as a member of the Árpádian Dynasty), access to expensive (luxury) and peculiar foods (e.g. seafood, shells and fish), even in the middle of the Carpathian Basin is probable. Despite the radiocarbon results, our multidisciplinary data thus support the early 20th century hypothesis of L. Bartucz that the investigated remains represent Béla, Duke of Macsó (4).

The IBD analysis verified that the individual in question is a fourth-degree descendant of King Béla III of Hungary from the Árpád dynasty, supporting the hypothesis that he was Duke Béla of Macsó. His ancestry, characterized by a mixture of medieval Scandinavian, Eastern Mediterranean, and Árpád-era Hungarian components, along with his Y-chromosomal lineages matching that of the Rurikid house, validates the hypothesis derived from historical data through whole-genome analyses.

The estimated age-at-death and osteological sex of the examined individual also correspond to expectations of Béla, Duke of Macsó, who was likely born c. 1245 and died in 1272.

The stable isotope results indicate that Béla of Macsó's diet was rich in C3 cereals (such as wheat and barley) and animal proteins, reflecting high social status. The dental calculus analysis further supports the consumption of wheat and barley, which fits into the known dietary patterns of medieval populations in the region (Supplementary Information 4) (26). The forensic traumatological investigation allowed us to reconstruct the circumstances of Duke Béla of Macsó's death. All his wounds are clearly caused by interpersonal aggression and a coordinated assault involving probably three assailants. The brutality of the attack, the encircling of the victim with strikes from three sides, and the character of blows show the intent to leave no chance of survival for the duke. The numerous poorly aimed attacks on the victim and the degree of damage to his face suggest a strong emotional involvement of hate and rage. Thus, while possibly premeditated and planned, the murder was not committed in cold blood.

Materials and Methods

This research complies with all relevant ethical regulations. While archaeological skeletal remains are not considered human subjects and thus are not covered by Human Subjects regulations, we obtained formal permission for analysis of all samples from local authorities (Department of Anthropology, Hungarian Natural History Museum; Department of Biological Anthropology, Institute of Biology, Faculty of Science, Eötvös Loránd University). All samples investigated were analyzed with the goal of minimizing damage.

Material

The skull (Figure 1) is housed in the Török Aurél Collection of Department of Biological Anthropology of the Faculty of Science at Eötvös Loránd University, while the postcranial bones (Supplementary Figure 2) are curated in the Hungarian Natural History Museum (Budapest, Hungary).

The preservation of the bones is generally good, though the lumbar spine, several phalanges, and ribs are missing. The bone surfaces exhibit minimal weathering; however, the skull interior showed extensive reconstructions from earlier treatments involving glue, paper, and plaster. The exterior mainly remained unchanged except for a possible varnish application, indicated by a visible surface shine.

Methods

Biological Anthropology, Forensic Anthropology

Sex, age, and stature were estimated following Brůžek et al. (27), Sjøvold (28), and by the Transition analysis (TA2) (29). Craniofacial bones were scanned using a dental CT scanner (3D Accuitomo-XYZ SliceView Tomograph; J. Morita, Japan).

All bones were examined for mechanical damage, and assessments were conducted to differentiate between antemortem, perimortem, and postmortem origins. The lesions were analyzed for forensic information using macroscopic and radiologic imaging inspections. Diagnostic marks on the damaged surfaces were scrutinized to determine directions, angles, probable movement vectors, and the likely positioning of the involved parties by fitting tool proxies to the lesions. Where possible, the sequence of wound infliction was determined based on overlapping or interruptions of fractures. All injuries were also mapped onto an assembled artificial skeleton, which was used to reconstruct plausible poses and positions of the victim and the directions of the attacks (30, 31).

Radiocarbon, stable carbon, nitrogen and strontium isotope investigations The collagen fraction of the selected bone samples, devoted to ¹⁴C and stable carbon and nitrogen isotope measurements, was prepared and measured at the HUN-REN Institute for Nuclear Research, Debrecen (32, 33). Prior to the AMS ¹⁴C analysis, samples from a rib and the occipital bone were taken. For control measurement, a sample was delivered to the University of Georgia, United States. As some influence of contamination originating from preservatives was assumed, various pretreatment protocols were suggested and tested for purification of the bones. These ranged from the modified Longin method through ultrafiltration (VIVASPIN 15R, 30,000 MWCO HY) to a complex treatment consisting of all the physical and chemical steps, supplemented with Soxhlet-extraction (33). In one case, the outer and inner layers of the bone were also separated and pretreated independently. For measurement, a small aliquot of freeze-dried gelatin obtained from each sub-sample was combusted with MnO2 reagent and the CO2 was then purified and graphitized. The bioapatite fraction of the rib was pretreated in the laboratory according to the standard protocol of cremated bones, i.e. after chemical cleaning, the structural carbonate of the inorganic part was extracted by adding 5 ml 85% orthophosphoric acid.

The AMS analysis of graphites was performed by the EnvironMICADAS AMS instrument at the INTERACT laboratory (34). As control organic samples, a blank bone (Ursus spelaeus bone with infinite ¹⁴C age) and internal standard bone (Bos primigenius prim. tibia from the Early Neolithic) was also applied for blank correction and checking the feasibility of the preparation process. In the case of the bioapatite measurement, international IAEA C1 (marble) and C2 (travertine) standards were applied. For the calibration and testing the possible freshwater reservoir effect (as deltaR shifts of the years) of the samples, the OxCal software (v4.4) (35) was used and the IntCal20 radiocarbon calibration curve was considered (36, 37). The calibrated date ranges are reported with 2σ probability range.

For stable carbon and nitrogen isotope ratio analysis, repeated aliquots from the same gelatinized collagens produced by the different cleaning methods were combusted in ultraclean aluminum cups using an elemental analyzer interface (Thermo ScientificTM, EA IsoLink CNSOH). Control measurements of IAEA 600 (caffeine) international, in addition, sulphanilamide laboratory standards were applied for calibration of the $\delta13C$ and $\delta15N$ values (33). The stable isotope ratios were measured using a Thermo Finnigan Delta Plus XP isotope ratio mass spectrometer. Repeated measurements were applied to achieve the precision of $\pm0.2\%$.

Strontium (Sr) sample solutions for isotope ratios were measured by a Neptune Plus MC-ICP-MS (Thermo Scientific) equipped with an Aridus-3 (CETAC) desolvating nebuliser system (dry plasma) at ICER) (38). The raw measurement data were normalized to a standard solution of 35 ppb prepared from the NIST SRM987 international Sr standard (Nat. Inst. of Stand. and Techn.). The 87Sr/86Sr ratio was corrected for instrumental mass discrimination using 88Sr/86Sr = 8.375209, as well as by applying an interference correction for 87Rb+ and 86Kr+ with 85Rb+ and 83Kr+, respectively. All values were normalized to the reported value of 0.710248 for NIST SRM 987 (38).

Genetic Testing

The laboratory work for genetic testing was carried out at the Institute of Archaeogenomics, HUN-REN Research Centre for the Humanities (Budapest, Hungary), and the Department of Genetics, Harvard Medical School, after the sample preparation at the Department of Evolutionary Anthropology of the University of Vienna.

Laboratory work

The whole genome capture and sequencing was done at the Laboratory of the Harvard Medical School.

Sampling (Budapest)

The sample BPDOM01 was drilled from the left petrous part of the temporal bone from the basis of the intact skull.

DNA extraction for the uniparental analysis, STR analysis, library preparation for mitocapture (Budapest)

DNA was extracted from petrous bone powder using established protocols in Budapest and Harvard, incorporating laboratory-specific modifications. All operations for the uniparental investigations were conducted within the dedicated ancient DNA laboratory of the Institute of Archaeogenomics, Research Centre for the Humanities, HUN-REN in Budapest, Hungary.

DNA extraction followed the procedure outlined by Dabney et al. (39), with minor adjustments as highlighted by Lipson et al. (40) from 50 mg bone powder. DNA library

preparation involving partial (half) uracil-DNA-glycosylase treatment followed the protocol outlined in Rohland et al. (41), with slight adjustments. Partially double-stranded and barcoded P5 and P7 adapters were employed. Amplification of the libraries was conducted using TwistAMP (TwistDX). The resulting amplification products were purified using AMPure Beads Purification (Agilent). For capturing target sequences encompassing the entire mitochondrial genome an in-solution hybridization method was adopted, as described by Csáky et al. (42) The captured samples were indexed using universal iP5 and unique iP7 indexes. Next-generation sequencing was conducted utilizing the Illumina MiSeq System (Illumina) employing V3 (2 × 75 cycles) sequencing kits. The AmpFISTR® Yfiler® PCR Amplification Kit (Applied Biosystems) was used to investigate the short tandem repeats (STRs) of the Y-chromosome, starting the reaction from the DNA extract (42), and typing 17 STR markers. Three independent reactions resulted in an STR profile.

DNA extraction and library preparation for the whole genome capture and sequencing (Harvard)

Bone powder was prepared from cochlea at Pinhasi Lab, Vienna following the Pinhasi et al. (43) method. DNA was extracted from 35 mg of powder using an automated ('robotic') procedure using silica magnetic beads and Dabney Binding Buffer on the Agilent Bravo NGS workstation (44). USER-treated single-stranded library was produced using automation and then enriched in-solution for sequences overlapping 1.24 million SNPs. (45, 46). The sequencing platform for 1240k capture data was Illumina HiSeq X10, 2x101 bp read length.

Bioinformatic data analysis

We processed the raw mitogenome sequence data using the same in-house pipeline outlined in Gerber et al. (23), utilizing the PAPline package with default settings (47). The sample underwent sequencing in Harvard Laboratory to produce raw paired-end reads. Paired-end reads were merged into single-molecule sequences based on overlapping regions. Single-end reads were aligned to the hg19 human reference genome (48) and the Reconstructed Sapiens Reference Sequence (RSRS) mitochondrial genome using the samse aligner of BWA. Duplicate molecules were identified and marked based on barcoding bins, start/stop positions, and orientation. The computational workflows, along with the specific parameters used, are publicly available on GitHub: ADNA-Tools and adna-workflow.

For variant calling, a pseudo-haploid approach was applied to targeted SNPs, wherein a single base was randomly selected from the possible alleles at each position. Filtering criteria included a minimum mapping quality of 10 and a base quality of 20, with additional trimming of two base pairs from both the 5' and 3' ends of reads to mitigate damage-related artifacts.

The ratio of male X-chromosomal contamination was measured, with both ANGSD (version 0.939-10-g21ed01c, htslib 1.14-9-ge769401) (49) and hapCon (hapROH package version 0.60) (50). All parameters used in both methods were the default settings recommended in the official documentation. The starting file for the former method was a samtools mpileup (version 1.10, htslib 1.10.2-3ubuntu0.1) output with mapping quality 25 and base quality 30. ANGSD doCounts was run on the X-chromosomal region from position 5500000 to 154000000, with mapping and base qualities 25 and 30 respectively. Contamination levels of the mtDNA were estimated using the ContamMix software (46), for results, see Supplementary Table 7. The mtDNA haplogroup was determined by Haplogrep (51, 52). For mitochondrial phylogenetic analysis, method described in Csáky

et al. (42) was followed, using all known and available sequences assigned to U3 haplogroup, keeping only the U3b3 sub branch (Supplementary Table 3).

The STR data analysis was carried out with GeneMapper® ID Software v3.2.1 (Applied Biosystems). To examine the STR variation within the Y-chromosomal haplogroup, Median Joining (MJ) network was constructed using the Network 10.2.0.0 program and the figure was drawn with the Network Publisher 2.1.2.5 program. The DYS385 locus was excluded because the Network program cannot handle the duplicated loci (DYS385a, DYS385b).

Yleaf (53) was applied for Y-chromosomal haplogroup inference from next generation sequencing data (Supplementary Table 2). Imputation was done with the GLIMPSE1 software suite (54). During the process, we mainly followed the developers' official GRCh37 tutorial (55), and used the v1.1.1 versions of the precompiled static binaries distributed on github (56).

The reference panel used was the 1000 Genomes Project (30X from NYGC) on hg19/GRcH37. Genotype likelihoods of the samples were computed with a standard method involving bcftools mpileup and bcftools call (version 1.10.2). Base- and mapping quality (flags -Q and -q) were both set to 20. As a difference from the official workflow, chromosomal level imputation regions were determined on a per sample basis, with the GLIMPSE_chunk_static executable, using default parameters (--window-size 2000000 --buffer-size 200000).

To identify identity by descent segments among samples we used ancIBD (version 0.5) (19) with the same process and parameters described in the software's official documentation (57).

Nuclear variants with clinical significance and pigmentation variants were analysed with the variant calling tool from the PAPline package (23). The panel contains 18738 variants, of which 61 are pigmentation markers, and the rest are clinically relevant positions.

Dental calculus microremain analysis

First, the teeth were visually investigated to acquire information about the diet from the dental plaque. During the sample-collecting process, powder-free gloves were worn in starch-free conditions. The series of teeth in the jaw and the spaces between the teeth were thoroughly brushed with an original hard bristle toothbrush to remove the modern contamination using ultra-pure water (UPW). The large deposits of calculus were carefully removed with a dental tool. After cleaning, the samples were processed based on King et al. (58). Retrieved calculus fragments were placed in 2 ml Eppendorf tubes, and 1 ml 10% hydrochloric acid was added to dissolve the matrix of the calculus fragments and release microremains. Stirring in acid solution lasted until no more calculus fragments were visible (15 min to 2 hours), and samples were centrifuged at 3000 rpm for 5 min. The supernatant was pipetted out, and after adding UPW, the tube was centrifuged three times. Finally, ethanol was added, and after centrifugation and pipetting out the supernatant, the samples were dried at 30 °C. The powder-like samples were resolved by adding 20 ml of immersion oil and vortexed. The suspension was dropped on slides and the cover slips were fixed with clear nail polish. Microremains were photographed and identified under a Nikon Eclipse polarizing light microscope at a magnification 400x. The microremains found in the dental calculus were compared with the research site's reference microremains database (Isotope Climatology and Environmental Research Centre, Hungary). Microphotos of the samples were archived with laboratory code ML207245.

References

523524

525

526

527

528

529530

531

532

533

534

535

536

537

538

539

540

541

542

543

544

545

546

547

548

549

550

551

552

553

554

555

556

557

558

559

560

561

562563

564

565

566

567

568569

570

571

Kádár T. Egy rejtélyes politikai gyilkosság és háttere a XIII. század végi Magyarországon:

- Béla macsói és boszniai herceg pályája (A mysterious political murder and its background in late thirteenth-century Hungary: the career of Duke Béla of Macsó and Bosnia). *Fons* **14**, 411–429 (2009).
 - 2 Salkovics K. Magyar Építészeti Múzeum és Műemlékvédelmi Dokumentációs Központ MÉM MDK (Hungarian Museum of Architecture and Monument Protection Documentation Center) 1915; 226. MDK 226/1915.
- Árpádházi Béla herceg sírjánál. Lux Kálmán és Bartucz Lajos ásatásai a Margitszigeten (Excavations at the tomb of Prince Béla of Árpádháza by Kálmán Lux and Lajos Bartucz on Margaret Island). *Magyarság* **141**, 5 (1922).
- Bartucz L. *Magyar föld magyar faj IV.: A magyar ember A magyarság antropológiája*. (Királyi Magyar Egyetemi Nyomda, Budapest, 1938).
 - 5 Buzár Á, Bernert Zs. Macsói Béla Árpád-házi herceg emberi maradványainak vizsgálata. *Annls Mus. hist.-nat. hung* **111**, 203–214 (2019).
 - 6 Leonard C, Vashro L, O'connell JF, Henry AG. Plant microremains in dental calculus as a record of plant consumption: A test with two forager-horticulturalists. *J. Archaeol. Sci. Rep.* **2**, 449–457 (2015). https://doi.org/10.1016/j.jasrep.2015.03.009
 - Henry AG, Hudson HF, Piperno DR. Changes in starch grain morphologies from cooking. *J. Archaeol. Sci.* **36(3)**, 915–922 (2009). https://doi.org/10.1016/j.jas.2008.11.008
- MacKenzie L, Speller CF, Holst M, Keefe K, Radini A. Dental calculus in the industrial age: Human dental calculus in the Post-Medieval period, a case study from industrial Manchester. *Quat. Int.* **653–654**, 114–126 (2023). https://doi.org/10.1016/j.quaint.2021.09.020
- 594 9 Departmentier MLC, Kempf M, Bánffy E, Alt KW. Tracing Mobility Patterns through the 595 6 6th-5th Millennia BC in the Carpathian Basin with Strontium and Oxygen Stable Isotope 596 Analyses. *PLoS One* **15(12)**, e0242745 (2020). 597 https://doi.org/10.1371/journal.pone.0242745. eCollection 2020.
 - Schoeninger MJ, DeNiro MJ, Tauber H. Stable nitrogen isotope ratios of bone collagen reflect marine and terrestrial components of prehistoric human diet. *Science* **220(4604)**, 1381–1383 (1983). https://doi.org/10.1126/science.6344217
 - 11 https://www.familytreedna.com/public/rurikid?iframe=ydna-results-overview
- Zhur KV, Sharko FS, Sedov VV, Dobrovolskaya MV, Volkov VG, Maximov NG et al.
 The Rurikids: The first experience of reconstructing the genetic portrait of the ruling family of Medieval Rus' based on paleogenomic data. *Acta Naturae* **15(3)**, 50–65 (2023). https://doi.org/10.32607/actanaturae.23425
- 606 13 yfull.com/mtree/

576

577

583

584

585

586

587

588

589

598

599

600

- Agranat-Tamir L, Waldman S, Martin MAS, Gokhman D, Mishol N, Eshel T. et al. The Genomic History of the Bronze Age Southern Levant. *Cell* **181(5)**, 1–146-1157.e11 (2020). https://doi.org/10.1016/j.cell.2020.04.024.
- Margaryan A, Derenko M, Hovhannisyan H, Malyarchuk B, Heller R, Khachatryan Z, et al. Eight Millennia of Matrilineal Genetic Continuity in the South Caucasus. *Curr Biol.* **27(13)**, 2023–28.e7 (2017). https://doi.org/10.1016/j.cub.2017.05.087.
- Mallick, S., Reich, D. *The Allen Ancient DNA Resource (AADR): A curated compendium* of ancient human genomes. (2023). https://doi.org/doi:10.7910/DVN/FFIDCW
- Jørsboe E, Hanghøj K, Albrechtsen A. fastNGSadmix: admixture proportions and principal component analysis of a single NGS sample. *Bioinformatics* **33**, 3148–3150. (2017). https://doi.org/10.1093/bioinformatics/btx474. https://github.com/e-jorsboe/fastNGSadmix
- Vyas DN, Koncz I, Modi A, Mende BG, Tian Y, Francalacci P, et al. Fine-scale sampling uncovers the complexity of migrations in 5th-6th century Pannonia. *Curr. Biol.* **33(18)**, 3951-61.e11 (2023). https://doi.org/10.1016/j.cub.2023.07.063.
- Ringbauer H, Huang Y, Akbari A, Mallick S, Olalde I, Patterson N, et al. Accurate

- detection of identity-by-descent segments in human ancient DNA. Nat. Genet. 56(1),143-622 151 (2024). https://doi.org/10.1038/s41588-023-01582-w. 623
- 20 Olasz J, Seidenberg V, Hummel S, Szentirmay Z, Szabados G, Melegh B, et al. DNA 624 profiling of Hungarian King Béla III and other skeletal remains originating from the Royal 625 Basilica of Székesfehérvár. Archaeol. Anthropol. Sci. 11, 1345–1357 (2019). 626 https://doi.org/10.1007/s12520-018-0609-7. 627
- 21 Wang CC, Posth C, Furtwängler A, Sümegi K, Bánfai Zs, Kásler M et al. Genome-wide 628 629 autosomal, mtDNA, and Y chromosome analysis of King Bela III of the Hungarian Arpad dynasty. Sci Rep 11, 19210 (2021). https://doi.org/10.1038/s41598-021-98796-x 630
- 22 Varga GIB, Kristóf LA, Maár K, Kis L, Schütz O, et al. The archaeogenomic validation of 631 Saint Ladislaus' relic provides insights into the Árpád dynasty's genealogy. J. Genet. 632 Genom. **50(1)**, 58–61 (2023). https://doi.org/10.1016/j.jgg.2022.06.008 633
- Gerber, D., Szeifert, B., Székely, O., Egyed, B., Gyuris, B., Giblin, J.I. et al. 23 634 Interdisciplinary Analyses of Bronze Age Communities from Western Hungary Reveal 635 Complex Population Histories. Mol. Biol. Evol. 40(9), msad182 636 (2023). https://doi.org/10.1093/molbev/msad182 637
- 24 Schulting RJ, Ramsey CB, Bazaliiskii VI, Goriunova OI, Weber A. Freshwater Reservoir 638 Offsets Investigated Through Paired Human-Faunal 14C Dating and Stable Carbon and 639 Nitrogen Isotope Analysis at Lake Baikal, Siberia. Radiocarbon 56(3), 991–1008 (2014). 640 https://doi.org/10.2458/56.17963
 - Ervynck A, Boudin M, Van Neer W. Assessing the Radiocarbon Freshwater Reservoir 25 Effect for a Northwest-European River System (the Schelde Basin, Belgium). Radiocarbon 60(2), 395–417 (2018). https://doi.org/10.1017/RDC.2017.148
- Balassa I (ed.) Magyar Néprajz IV. Életmód. (Akadémiai Kiadó, Budapest, 1997). 26 645 http://mek.niif.hu/02100/02152/html/04/240.html 646

642

643

- 27 Brůžek J, Santos F, Dutailly B, Murail P, Cunha E. Validation and reliability of the sex 647 estimation of the human os coxae using freely available DSP2 software for bioarchaeology 648 and forensic anthropology. Am. J. Phys. Anthropol. 164(2), 440–449 (2017). 649 https://doi.org/10.1002/ajpa.23282 650
- Sjøvold T. Estimation of stature from long bones utilizing the line of organic correlation. 651 28 Hum. Evol. 5, 431–447 (1990). https://doi.org/10.1007/BF02435593 652
- 29 Boldsen JL, Milner GR, Konigsberg LW, Wood JW. Transition analysis: a new method for 653 estimating age from skeletons. In Paleodemography: Age Distributions from Skeletal 654 Samples (eds. Hoppa RD, Vaupel JW) pp. 73–106 (Cambridge University Press, 655 Cambridge, 2002). https://doi.org/10.1017/CBO9780511542428.005 656
- 30 Ogle RRJr. Crime Scene Investigation and Reconstruction. 2nd ed. (Prentice Hall, Upper 657 Saddle River, N.J., 2007). 658
- McCardle P, Stojanovski E, Identifying Differences Between Cut Marks Made on Bone by 31 659 a Machete and Katana: A Pilot Study. *J. Forensic. Sci.* **63(6)**, 1813–1818 (2018). 660 https://doi.org/10.1111/1556-4029.13754 661
- Molnár M, Rinyu L, Veres M, Seiler M, Wacker L and Synal H-A. EnvironMICADAS: a 32 662 mini 14C AMS with enhanced gas ion source interface in the Hertelendi Laboratory of 663 Environmental Studies (HEKAL), Hungary. Radiocarbon 55(2–3), 338–344 (2013). 664 https://doi.org/10.1017/S0033822200057453 665
- 33 Major I, Futó I, Dani J, Cserpák-Laczi O, Gasparik M, Jull TAJ, et al. Assessment and 666 development of bone preparation for radiocarbon dating at HEKAL. Radiocarbon 61. 667 1551–1561 (2019). https://doi.org/10.1017/RDC.2019.60 668
- Major I, Dani J, Kiss V, Melis E, Patay R, Szabó G, et al. Adoption and evaluation of a 34 669 sample pretreatment protocol for radiocarbon dating of cremated bones at HEKAL. 670 Radiocarbon 61(1), 159–171 (2019). https://doi.org/10.1017/RDC.2018.41 671

- 35 Bronk Ramsey C. Bayesian Analysis of Radiocarbon Dates. Radiocarbon 51(1), 337–360 672 (2009). https://doi.org/10.1017/S0033822200033865 673
- Reimer PJ, Austin WEN, Bard E, Bayliss A, Blackwell PG, Bronk Ramsey C. et al. The 674 36 IntCal20 Northern Hemisphere Radiocarbon Age Calibration Curve (0–55 cal kBP). 675 Radiocarbon 62(4),725–757. 2020; https://doi.org/10.1017/RDC.2020.41 676

681

682

683

684

685

686

687

688

689

690

691

692

693

699

701

702

703

- 37 Heaton TJ, Köhler P, Butzin M, Bard E, Reimer RW, Austin WEN, et al. Marine20—The 677 Marine Radiocarbon Age Calibration Curve (0-55,000 cal BP). Radiocarbon 62(4): 779-678 679 820 (2020). https://doi.org/10.1017/RDC.2020.68
 - 38 McArthur JM, Howarth RJ, Bailey TR. Strontium Isotope Stratigraphy: LOWESS Version 3: Best Fit to the Marine Sr-Isotope Curve for 0–509 Ma and Accompanying Look-up Table for Deriving Numerical Age. J. Geol. 109: 155–170 (2001). https://doi.org/10.1086/319243
 - Dabney J, Knapp M, Glocke I, Gansauge M-T, Weihmann A, Nickel B. et al. Complete 39 mitochondrial genome sequence of a Middle Pleistocene cave bear reconstructed from ultrashort DNA fragments. Proc. Natl. Acad. Sci. 110: 15758–15763 (2013). https://doi.org/10.1073/pnas.1314445110
 - 40 Lipson M, Szécsényi-Nagy A, Mallick S, Pósa A, Stégmár B, Keerl V, et al. Parallel palaeogenomic transects reveal complex genetic history of early European farmers. Nature **551**, 368–372 (2017). https://doi.org/10.1038/nature24476
 - 41 Rohland N, Harney E, Mallick S, Nordenfelt S, Reich D. Partial uracil-DNA-glycosylase treatment for screening of ancient DNA. Philos Trans R Soc Lond B Biol Sci. 370(1660), 20130624 (2015). https://doi.org/10.1098/rstb.2013.0624
- 42 Csáky V, Gerber D, Koncz I, Csiky G, Mende BG, Szeifert B, et al. Genetic insights into 694 the social organisation of the Avar period elite in the 7th century AD Carpathian Basin. Sci 695 Rep. 10(1), 948 (2020). doi: 10.1038/s41598-019-57378-8. Erratum in: Sci Rep. 10(1), 696 13398 (2020). https://doi.org/10.1038/s41598-020-69583-x. 697
- Pinhasi R, Fernandes D, Sirak K, Novak M, Connell S, Alpaslan-Roodenberg S, et al. 698 43 Optimal Ancient DNA Yields from the Inner Ear Part of the Human Petrous Bone. PLoS ONE 10(6): e0129102 (2015). https://doi.org/10.1371/journal.pone.0129102 700
 - 44 Rohland N, Glocke I, Aximu-Petri A, Meyer M. Extraction of highly degraded DNA from ancient bones, teeth and sediments for high-throughput sequencing. Nat. Protoc. 13, 2447— 2461 (2018). https://doi.org/10.1038/s41596-018-0050-5
- Gansauge MT, Aximu-Petri A, Nagel S, Mever M, Manual and automated preparation of 704 45 single-stranded DNA libraries for the sequencing of DNA from ancient biological remains 705 and other sources of highly degraded DNA. Nat Protoc. 15(8), 2279–2300 (2020). 706 https://doi.org/10.1038/s41596-020-0338-0 707
- Fu O, Meyer M, Gao X, Stenzel U, Burbano HA, Kelso J, et al. DNA analysis of an early 46 708 modern human from Tianvuan Cave, China, Proc. Natl. Acad. Sci. U. S. A. 110(6), 2223-709 2227 (2013). https://doi.org/10.1073/pnas.1221359110. 710
 - 47 https://github.com/ArchGenIn/papline, accessed on 15 April 2025
- 48 https://www.internationalgenome.org/category/grch37/ 712
- Korneliussen TS, Albrechtsen A, Nielsen R. ANGSD: Analysis of Next Generation 49 713 Sequencing Data. BMC Bioinformatics 15(1), 356 (2014). https://doi.org/10.1186/s12859-714 014-0356-4. 715
- 50 Huang Y, Ringbauer H. hapCon: estimating contamination of ancient genomes by copying 716 from reference haplotypes. *Bioinformatics* **38(15)**, 3768–3777 (2022). 717 https://doi.org/10.1093/bioinformatics/btac390 718
- 51 https://haplogrep.i-med.ac.at/, accessed on 15 April 2025 719
- Weissensteiner H, Pacher D, Kloss-Brandstätter A, Forer L, Specht G, Bandelt HJ, et al. 52 720
- HaploGrep 2: mitochondrial haplogroup classification in the era of high-throughput 721

- sequencing. Nucleic Acids Res. 44(W1), W58–63 (2016).
 https://doi.org/10.1093/nar/gkw233.
- Ralf A, González DM, Zhong K, Kayser M. Yleaf: software for human Y-chromosomal haplogroup inference from next generation sequencing data. *Mol. Biol. Evol.* **35(5)**, 1291–1294. https://doi.org/10.1093/molbev/msy032.
 - Rubinacci S, Ribeiro DM, Hofmeister RJ, Delaneau O. Efficient phasing and imputation of low-coverage sequencing data using large reference panels. *Nat. Genet.* **53**, 120–126 (2021). https://doi.org/10.1038/s41588-020-00756-0
 - 55 <u>https://odelaneau.github.io/GLIMPSE/glimpse1/tutorial_hg19.html</u>, accessed on 15 April 2025
- 732 56 https://github.com/odelaneau/GLIMPSE/tree/glimpse1/static_bins, accessed on 15 April 2025
 - 57 https://ancibd.readthedocs.io/en/latest/run ancIBD.html, accessed on 15 April 2025
 - King DJ, Searcy MT, Yost CL, Waller K. Corn, beer, and marine resources at Casas Grandes, Mexico: An analysis of prehistoric diets using microfossils recovered from dental calculus. *J. Archaeol. Sci. Rep.* 16: 365–379 (2017).
- 738 https://doi.org/10.1016/j.jasrep.2017.10.013.

728 729

730

731

734735

736

737

739 740

741

752

753

754

References cited in the Supplementary Information 1-4 and in the Supplementary Tables

- Henry AG, Hudson HF, Piperno DR. Changes in starch grain morphologies from cooking. *J. Archaeol. Sci.* **36(3)**, 915–922 (2009). https://doi.org/10.1016/j.jas.2008.11.008
- Mickleburgh HL, Pagán-Jiménez JR. New insights into the consumption of maize and other food plants in the pre-Columbian Caribbean from starch grains trapped in human dental calculus. *J. Archaeol. Sci.* **39**, 2468–2478 (2012). https://doi.org/10.1016/j.jas.2012.02.020
- MacKenzie L, Speller CF, Holst M, Keefe K, Radini A. Dental calculus in the industrial age: Human dental calculus in the Post-Medieval period, a case study from industrial Manchester. *Quat. Int.* **653–654**: 114–26. (2023). https://doi.org/10.1016/j.quaint.2021.09.020
 - 4 Li Y, Zhang G, Nan P, Yang J, Cao J, Ma Z. et al. Wine or Beer? A reinvestigation of residues from bronze vessels from the Beibai'e cemetery, Shanxi China. *Heritage Science* 11: 184 (2023). https://doi.org/10.1186/s40494-023-01012-4
- 755 5 Balassa I (ed.) *Magyar Néprajz IV. Életmód.* (Akadémiai Kiadó, Budapest, 1997). 756 http://mek.niif.hu/02100/02152/html/04/240.html
- Radini A, Nikita E, Buckley S, Copeland L, Hardy K. Beyond food: The multiple pathways for inclusion of materials into ancient dental calculus. *Am. J. Phys. Anthropol.* **162**, 71–83 (2017). https://doi.org/10.1002/ajpa.23147
- Power RC, Salazar-García DC, Wittig RM, Henry AG. Assessing use and suitability of scanning electron microscopy in the analysis of micro remains in dental calculus.
 J. Archaeol. Sci. 49, 160–169 (2014). https://doi.org/10.1016/j.jas.2014.04.016
- Horrocks, M., Nieuwoudt, M., Kinaston, R., Buckley, H., Bedford, S.Microfossil and Fourier Transform InfraRed analyses of Lapita and post-Lapita human dental calculus from Vanuatu, Southwest Pacific. *J. Roy. Soc. New Zealand* **44(1)**: 17–33 (2013). https://doi.org/10.1080/03036758.2013.842177
- Decke, U. Mikroskopische Untersuchung an geschälten und zerkleinertenÖlsamen und
 Nußkernen. Z Lebensm Unters Forch 174, 187–194 (1982).
 https://doi.org/10.1007/BF01079972

10 [Margitszigeti ásatások] [Fénykép] | Képcsarnok 770

778

779

780

781

782

783

784

785

786

787

788 789

790

791

792

793

794 795

796

797 798

799

801

- 11 Price TD, Knipper C, Grupe G, Smrcka V. Strontium isotopes and prehistoric human 771 migration: the Bell Beaker period in central Europe. Eur. J. Archaeol. 7: 9–40 (2024). 772 https://doi.org/10.1177/1461957104047992 773
- Depaermentier MLC, Kempf M, Bánffy E, Alt KW. Tracing Mobility Patterns through the 12 774 775 6th-5th Millennia BC in the Carpathian Basin with Strontium and Oxygen Stable Isotope Analyses. PLoS One 15(12): e0242745 (2020). 776 https://doi.org/10.1371/journal.pone.0242745. eCollection 2020. 777
 - 13 Cavazzuti C, Hajdu T, Lugli F, Sperduti A, Vicze M, Horváth A, et al. Human mobility in a Bronze Age Vatya 'urnfield' and the life history of a high-status woman. PLoS One 16, e0254360 (2021). https://doi.org/10.1371/journal.pone.0254360
 - 14 Agranat-Tamir L, Waldman S, Martin MAS, Gokhman D, Mishol N, Eshel T. et al. The Genomic History of the Bronze Age Southern Levant. Cell 181(5), 1–146-1157.e11 (2020). https://doi.org/10.1016/j.cell.2020.04.024.
 - Maár K, Varga GIB, Kovács B, Schütz O, Maróti Z, Kalmár T. et al. Maternal Lineages 15 from 10-11th Century Commoner Cemeteries of the Carpathian Basin. Genes 12(3), 460 (2021). https://doi.org/10.3390/genes12030460
 - Saag L, Laneman M, Varul L, Malve M, Valk H, Razzak MA, et al. The arrival of Siberian 16 ancestry connecting the Eastern Baltic to Uralic speakers further East. Curr Biol. 29(10), 1701–11.e16 (2019). https://doi.org/10.1016/j.cub.2019.04.026.
 - 17 Damgaard PB, Marchi N, Rasmussen S, Peyrot M, Renaud G, Korneliussen T. 137 ancient human genomes from across the Eurasian steppes. *Nature* 557(7705), 369–374 (2018). https://doi.org/10.1038/s41586-018-0094-2. Erratum in: Nature 563(7729), E16 (2018). https://doi.org/10.1038/s41586-018-0488-1.
 - Margaryan, A., Lawson, D.J., Sikora, M. et al. Population genomics of the Viking 18 world. Nature 585, 390–396 (2020). https://doi.org/10.1038/s41586-020-2688-8
 - 19 Veeramah KR, Rott A, Groß M, van Dorp L, López S, Kirsanow K, et al. Population genomic analysis of elongated skulls reveals extensive female-biased immigration in Early Medieval Bavaria. Proc. Natl. Acad. Sci. U. S. A. 115(13), 3494–3499 (2018). https://doi.org/10.1073/pnas.1719880115.
- Antonio ML, Gao Z, Moots HM, Lucci M, Candilio F, Sawyer S. et al. Ancient Rome: A 20 800 genetic crossroads of Europe and the Mediterranean. Science 366(6466), 708–714 (2019). https://doi.org/10.1126/science.aav6826. 802
- Lazaridis I, Alpaslan-Roodenberg S, Acar A, Açıkkol A, Agelarakis A, Aghikyan L. et al. 21 803 A genetic probe into the ancient and medieval history of Southern Europe and West Asia. 804 Science 377(6609), 940–951 (2022). https://doi.org/10.1126/science.abq0755. 805
- 22 Maróti Z, Neparáczki E, Schütz O, Maár K, Varga GIB, Kovács B, et al. The genetic origin 806 of Huns, Avars, and conquering Hungarians. Curr Biol 32(13), 2858-70.e7 (2022). 807 https://doi.org/10.1016/j.cub.2022.04.093. 808
- Gerber D, Csáky V, Szeifert B, Borbély N, Jakab K, Mező Gy, et al. Ancient genomes 23 809 reveal Avar-Hungarian transformations in the 9th-10th centuries CE Carpathian Basin. Sci. 810 Adv. 10:eadq5864 (2024). https://doi.org/10.1126/sciadv.adq5864 811

Acknowledgments

We thank the National Centre for Biodiversity and Gene Conservation (Hungary) and the Research Institute of Karcag (Hungary) for plant reference material.

Funding:

The Hungarian Research, Development and Innovation Office FK142894 (ZSLSZ)

The Bolyai Scholarship of the Hungarian Academy of Sciences - project id: BO-783-22-8 (TH)

The Bolyai Scholarship of the Hungarian Academy of Sciences - project id: BO-710-23-10 (IM)

The Bolyai Scholarship of the Hungarian Academy of Sciences - project id: BO-357-23-10 (ZSLSZ).

Project No. KDP-2023-C2284509 has been implemented with the support provided by the Ministry of Culture and Innovation of Hungary from the National Research, Development and Innovation Fund, financed under the 2023-2.1.2-KDP-2023-00002 funding scheme (TH)

European Union and the State of Hungary, co-financed by the European Regional Development Fund (project of GINOP-2.3.4-15-2020-00007 "INTERACT") (IM).

The "MALTHUS" project, funded by the Italian Ministry of University and Research (PRIN2022: 2022ELZECR) (CC)

The Hungarian Natural History Museum and the House of Árpád Programme (2018–2023) Scientific Subproject: V.1. Anthropological-Genetic portrayal of Hungarians in the Árpádian Age (TH, TSZ, ZSB, ÁB)

The EKÖP-24-3-II university excellence scholarship program of the Ministry for Culture and Innovation from the source of the National Research, Development and Innovation Fund. ID: EKÖP-24-3-II-ELTE-474 (NB)

John Templeton Foundation Grant 61120 (DR)

Author contributions:

Conceptualization: TH, TSZ, IM, ÁT, ASZN

Methodology: TH, TSZ, TM, IM, ÁT, NB, AH, LP, BÁK, JA, BGM, ZSLSZ, DER, ASZN

Investigation: TH, NB, ZSB, ÁB, TSZ, IM, MM, AH, LP, BÁK, JA, BGM, ZSLSZ, ÁT, OC, RP, DER, MT, ASZN

Visualization: TH, NB, TSZ, IM, CC, MM, AH, BÁK, JA, ZSLSZ, ÁT, DER, MT, ASZN

Supervision: TH, NB, MT, ASZN.

Writing – original draft: TH, NB, IM, CC, AH, BÁK, JA, ZSLSZ, ÁT, RP, DER, MT, ASZN

Writing – review & editing: TH, NB, IM, CC, AH, BÁK, JA, ZSLSZ, ÁT, RP, DER, MT, ASZN

Competing interests:

The authors declare that they have no competing interests.

Data and materials availability:

The results of the biological anthropological, radiocarbon, stable isotope, dental calculus microremain analysis are available in the main text and in the supplementary materials. The ancient genome sequence of the BPDOM01 sample has been uploaded to ENA

(European Nucleotide Archive), under the accession number PRJEB92396.

Data required to generate all figures in the manuscript are available in the main text and in Supplementary materials.

Figures Legends

- Figure 1. The skull of the investigated individual from the 13th century Dominican monastery on Margaret Island, Budapest.
- Figure 2. The observed perimortem lesions on the human remains. The description of the traumatic alterations can be found in Supplementary information 1.1 and 1.2. CL=cranial lesion, PL= Postcranial lesion. The drawing of the skeleton was generated using OpenAI's image generation tools (DALL·E) via ChatGPT.
- Figure 3. Perimortem lesions on the frontal (A) and left parietal (B) bones caused by sharp weapons. White arrows show the sharp edges of the traumatic alterations without healing. The description of the traumatic alterations can be found in Supplementary information 1.1. CL=Cranial Lesion
- Figure 4. Perimortem cut-marks on the postcranial bones. White arrows show the sharp edges of the traumatic alterations without signs of healing. A: Perimortem cut marks on the spinous process of the 7th thoracic vertebra (PL14). B: Perimortem cut marks on the 10-11th thoracic vertebrae. The tip of the tool went from behind through the vertebral canal and was stopped by the vertebral body of the 11th thoracic vertebra (PL15). C: Perimortem cut marks on the anterolateral surface of the left tibia (PL8, PL9). D: Perimortem cut marks on the anterolateral surface of the left femur (PL10, PL11, PL12). The description of the traumatic alterations can be found in Supplementary information 1.2. PL=Postcranial Lesion
- Figure 5. Phylogenetic networks of the uniparental lineages of sample BPDOM01. Part A: Median Joining Network based on 11 Y-STR data of the closest N1a-L550 individuals' clusters from the Rurikids project. The closest individuals to BPDOM01 on the Median Joining Y network are derived for the SNP L550, but ancestral for the L1025 marker. Most of them are located under the VL15 and Y10931 "Rurikid" branches on the N phylogenetic tree, downstream from L550. Part B: Part of the U3 mitochondrial phylogenetic tree, showing the entire U3b3 branch. On the U3b3 tree, the most closely related lineages to the BPDOM01 sample are from present-day Armenia and the north-western Caucasus.
- Figure 6. European PCA and supervised genomic ancestry proportions of BPDOM01. A: PCA results with genotypes from medieval European populations. 560k SNPs were used for the calculations, performed in the smartpca program. The scatterplot was generated in R. B: fastNGSadmix analysis with an ancient reference panel following the concept presented at Vyas et al. (18)
- Figure 7. Degree of relationship vs IBD sharing and IBD sharing with known medieval personals from Hungary and Russia. Fig. 5A: Degree of relationship on simulated data with IBD sharing segments. Fig. 5B: Karyotype Plot of IBD sharing segments. This function of ancIBD depicts IBD between a pair of individuals along their chromosomes. The simulated data for comparison of relatedness were gained from Ringbauer et al. (19)

Figures

908

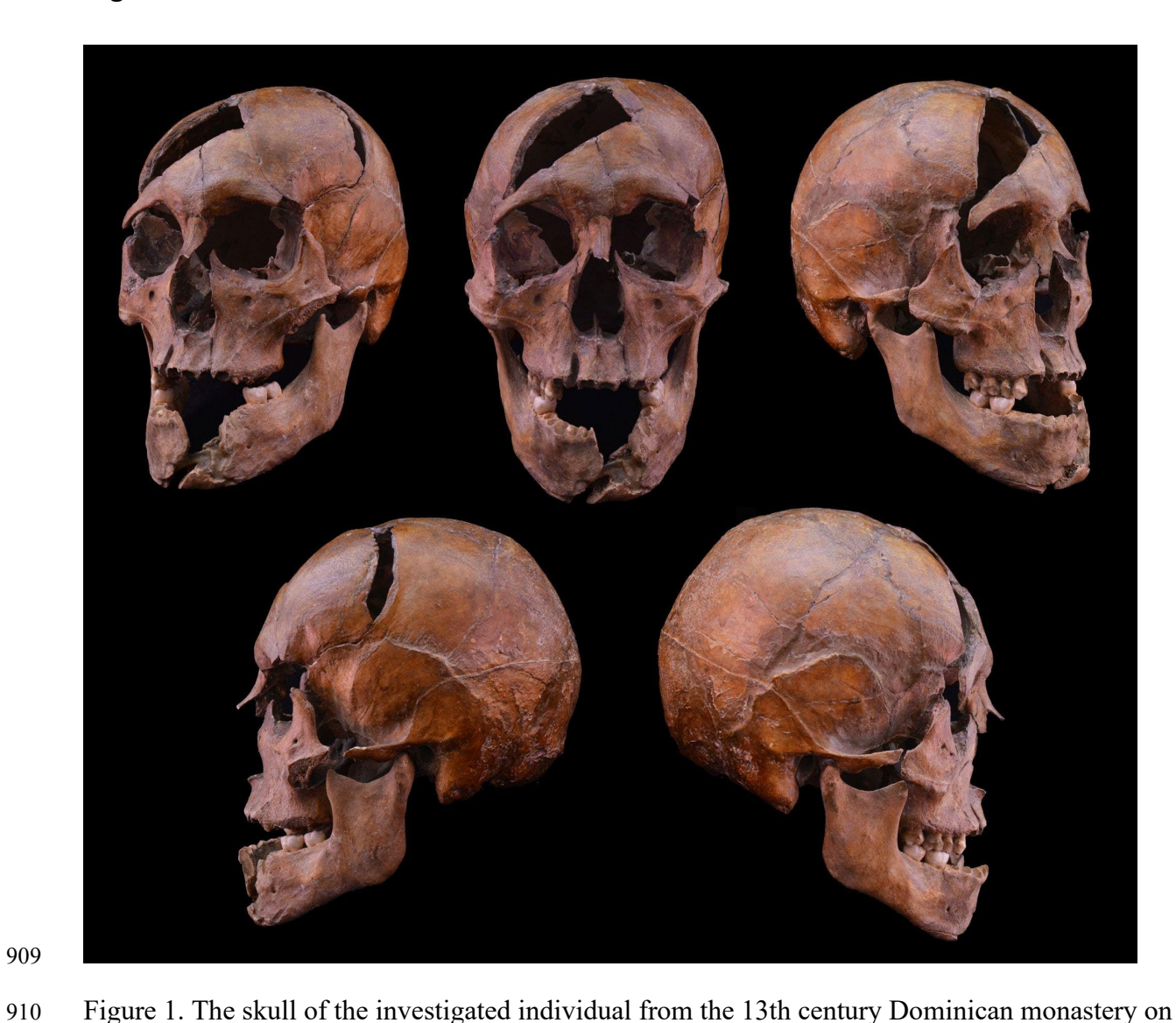


Figure 1. The skull of the investigated individual from the 13th century Dominican monastery on Margaret Island, Budapest.

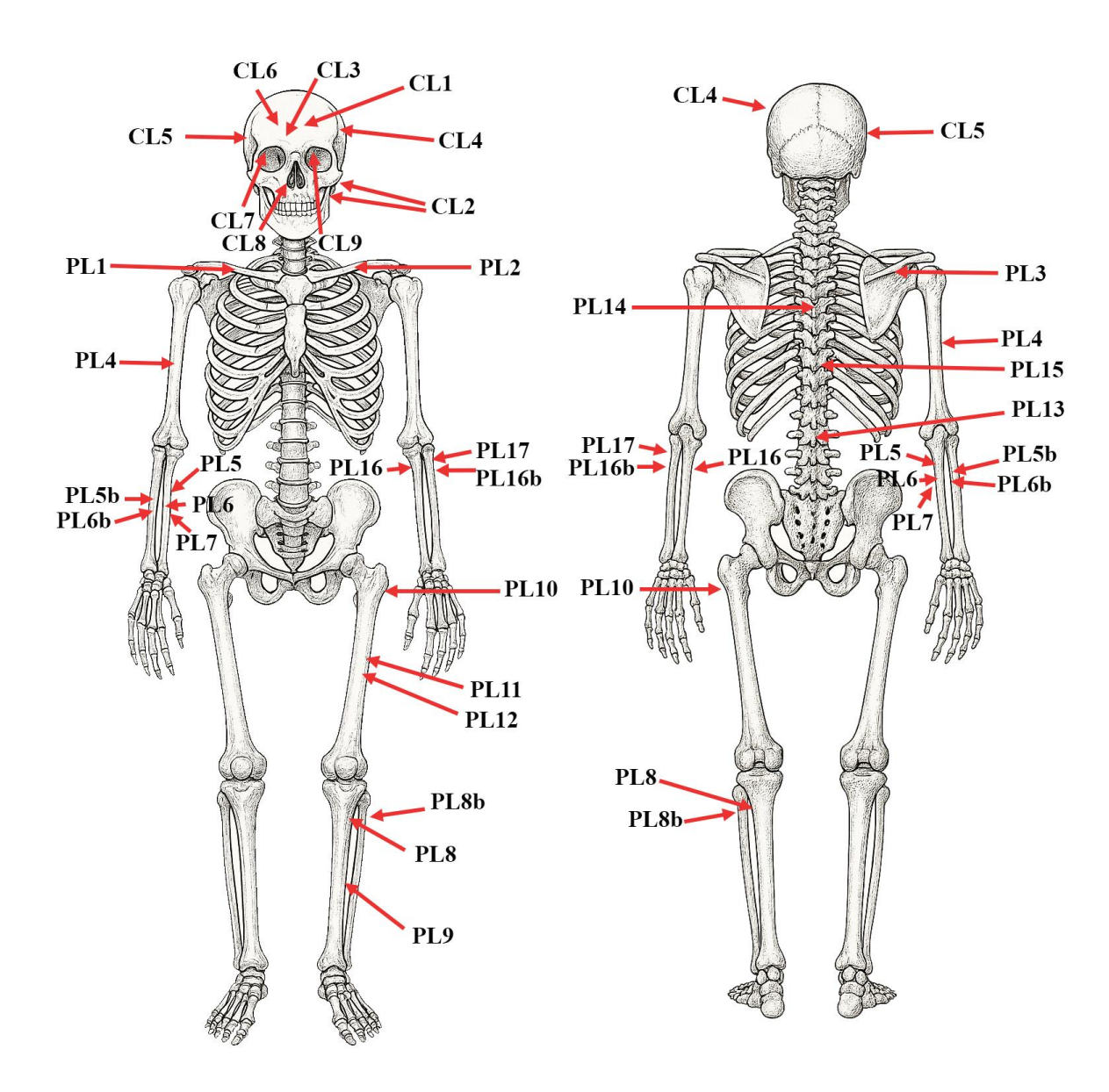


Figure 2. The observed perimortem lesions on the human remains. The description of the traumatic alterations can be found in Supplementary information 1.1 and 1.2. CL=cranial lesion, PL= Postcranial lesion. The drawing of the skeleton was generated using OpenAI's image generation tools (DALL·E) via ChatGPT.



Figure 3. Perimortem lesions on the frontal (A) and left parietal (B) bones caused by sharp weapons. White arrows show the sharp edges of the traumatic alterations without healing. The description of the traumatic alterations can be found in Supplementary information 1.1. CL=Cranial Lesion

947

948

949

950

951

952

953

954

955

956

Figure 4. Perimortem cut-marks on the postcranial bones. White arrows show the sharp edges of the traumatic alterations without signs of healing. A: Perimortem cut marks on the spinous process of the 7th thoracic vertebra (PL14). B: Perimortem cut marks on the 10-11th thoracic vertebrae. The tip of the tool went from behind through the vertebral canal and was stopped by the vertebral body of the 11th thoracic vertebra (PL15). C: Perimortem cut marks on the anterolateral surface of the left tibia (PL8, PL9). D: Perimortem cut marks on the anterolateral surface of the left femur (PL10, PL11, PL12). The description of the traumatic alterations can be found in Supplementary information 1.2. PL=Postcranial Lesion

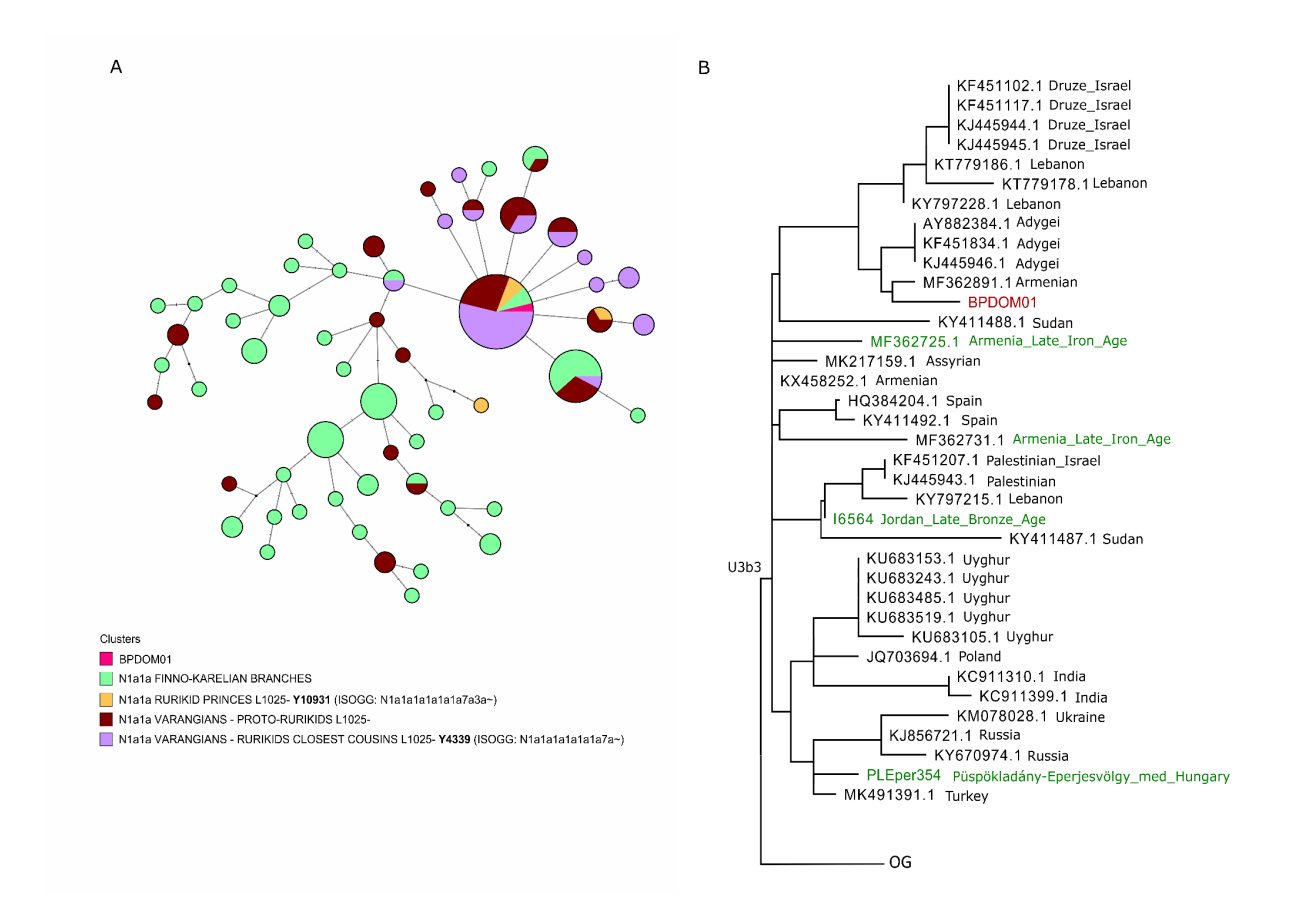


Figure 5. Phylogenetic networks of the uniparental lineages of sample BPDOM01. Part A: Median Joining Network based on 11 Y-STR data of the closest N1a-L550 individuals' clusters from the Rurikids project. The closest individuals to BPDOM01 on the Median Joining Y network are derived for the SNP L550, but ancestral for the L1025 marker. Most of them are located under the VL15 and Y10931 "Rurikid" branches on the N phylogenetic tree, downstream from L550. Part B: Part of the U3 mitochondrial phylogenetic tree, showing the entire U3b3 branch. On the U3b3 tree, the most closely related lineages to the BPDOM01 sample are from present-day Armenia and the north-western Caucasus.

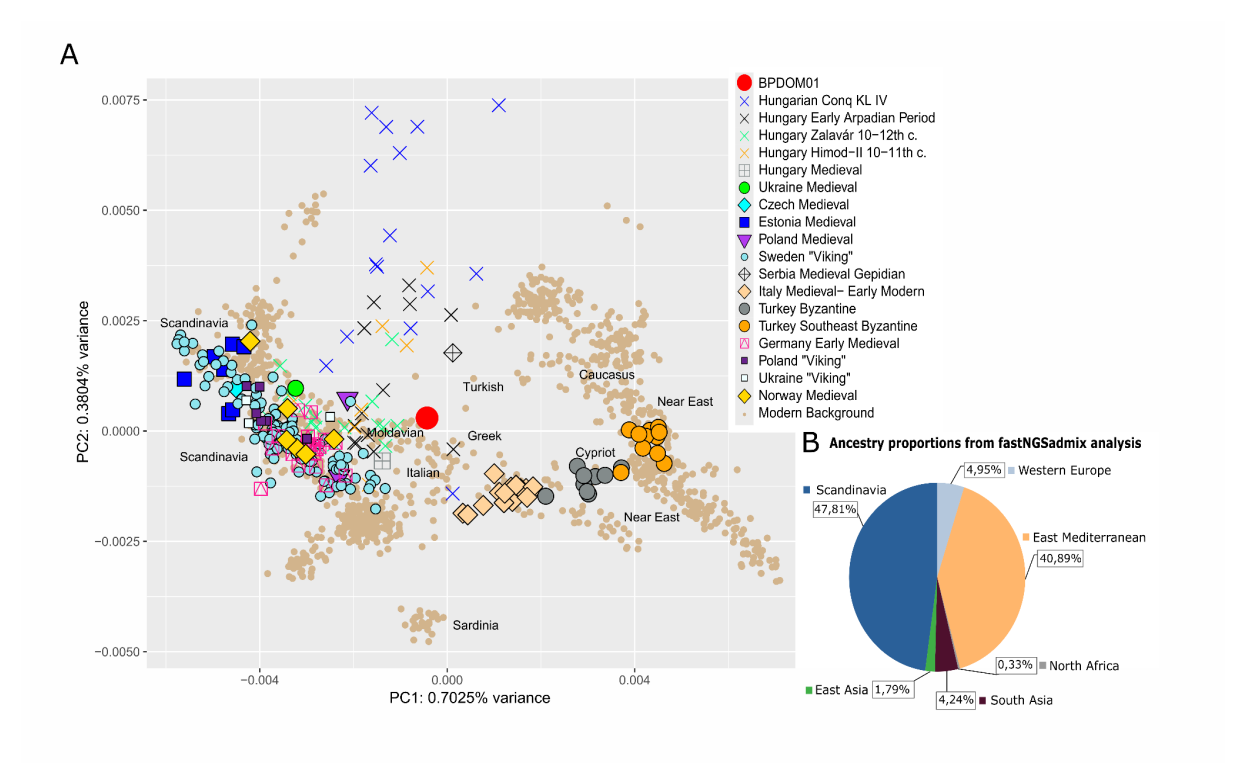


Figure 6. European PCA and supervised genomic ancestry proportions of BPDOM01. A: PCA results with genotypes from medieval European populations. 560k SNPs were used for the calculations, performed in the smartpca program. The scatterplot was generated in R. B: fastNGSadmix analysis with an ancient reference panel following the concept presented at Vyas et al. (18)

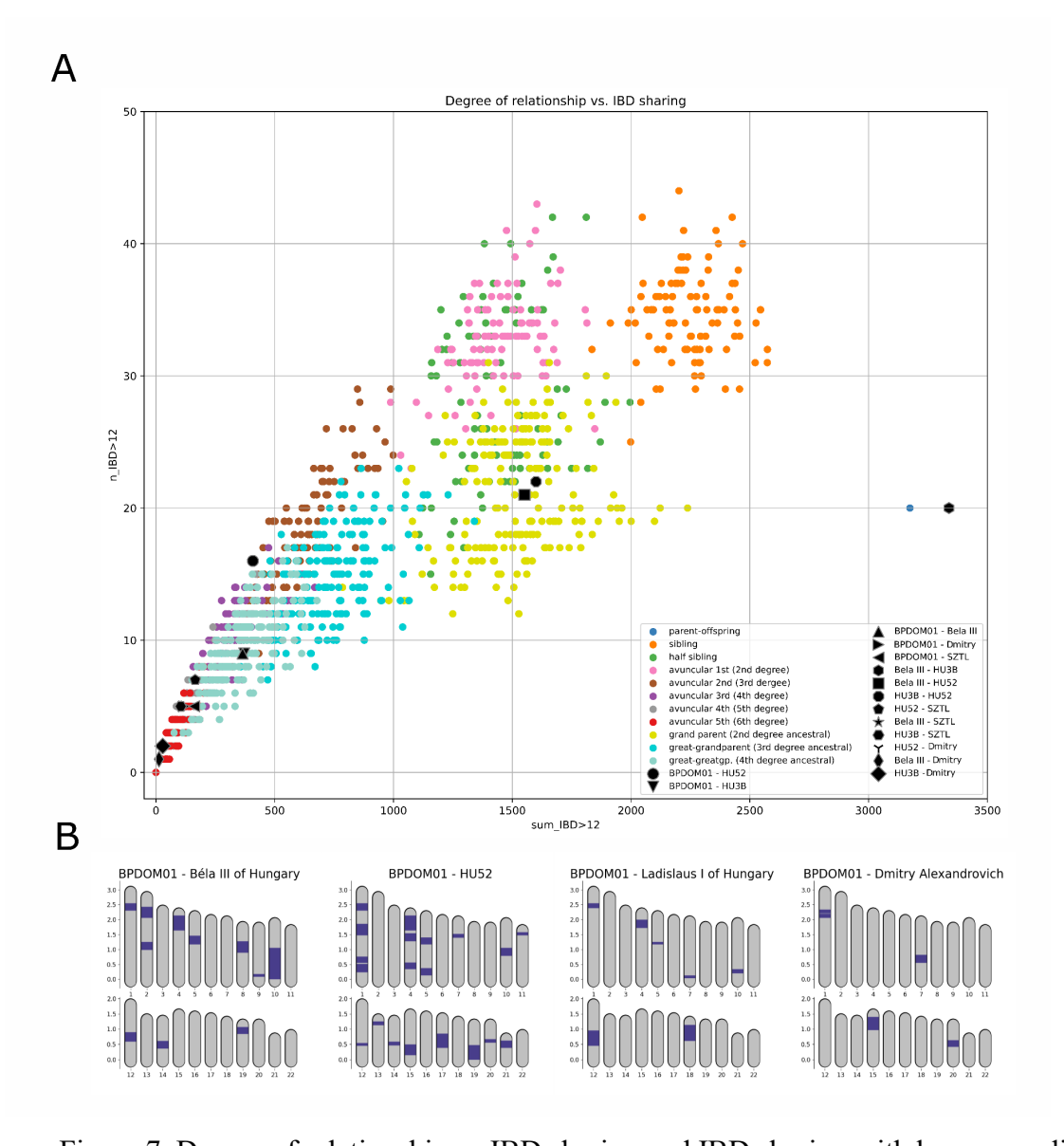


Figure 7. Degree of relationship vs IBD sharing and IBD sharing with known medieval personals from Hungary and Russia. Fig. 5A: Degree of relationship on simulated data with IBD sharing segments. Fig. 5B: Karyotype Plot of IBD sharing segments. This function of ancIBD depicts IBD between a pair of individuals along their chromosomes. The simulated data for comparison of relatedness were gained from Ringbauer et al. (19)